

Single-shot quantum measurements sketch quantum many-body states

Jia-Bao Wang and Yi Zhang*

International Center for Quantum Materials, School of Physics, Peking University, Beijing, 100871, China

Quantum measurements are our eyes to the quantum many-body systems consisting of a multitude of microscopic degrees of freedom. However, the quantum uncertainty and the exponentially large Hilbert space pose natural barriers to simple interpretations of the quantum measurement outcomes. We propose a nonlinear “measurement energy” based upon the measurement outcomes and a general approach akin to quantum machine learning to extract the most probable states (maximum likelihood estimates), naturally reconciling non-commuting observables and getting more out of the quantum measurements. We showcase the versatility and accuracy of our strategy on random long-range fermion and Kitaev quantum spin liquid models, where smoking-gun signatures were lacking.

Introduction —Quantum many-body systems exhibit fascinating yet elusive quantum phenomena, such as quantum fluctuations, strong correlations [1], quantum entanglements [2–9], quantum anomalies [10–15], with no counterpart in the macroscopic world [16]. For example, nontrivial spin and electronic systems like quantum spin liquid (QSL) [17–20], superconductors [21–24], topological phases [11, 12, 25–33], form a modern-day scientific cornerstone. While scientists have made much progress and established physical pictures that are simple and beautiful, it is common that we scratch our heads over their complex behaviors when encountering the vast and intertwined microscopic or emergent degrees of freedom [34, 35].

Experiments on quantum many-body systems are our window to their microscopic worlds. However, analysis of quantum measurements is intrinsically difficult due to quantum fluctuations that whenever a general observable $\hat{O} = \sum_{\gamma} a_{\gamma} \hat{P}_{\gamma}$ is measured, the outcome stochastically picks one of the a_{γ} eigenvalues with probability $\langle \hat{P}_{\gamma} \rangle$ [36]. Fortunately, if we measure the target state repeatedly, through either identical copies or relaxation, the resulting average converges to a non-stochastic and more physically interpretable expectation value $\langle \hat{O} \rangle$ [36]. We may further facilitate the investigation with a phenomenological picture or microscopic model, whose predictions offer smoking-gun signatures that we can compare with the quantum measurements. However, by presuming a model or picture, we not only waste seemingly unrelated data but also risk biases consciously or unconsciously. In addition, exotic quantum matters such as QSLs lack definitive signatures, compelling scientists to resort to a negative-evidence stance [19, 37] that may remain controversial and less controlled to a degree.

In this letter, we discuss a general strategy to determine the most probable quantum many-body states given the quantum measurement data. We interpret the quantum measurements as nonlinear measurement energy and offer an iterative effective-Hamiltonian strategy to obtain the Hilbert space’s maximum likelihood estimate (MLE) states, which in turn, provide us with all information,

including those unachievable directly, such as quantum entanglements [2–9] and topological characters [7–11]. In this way, we can utilize all measurement outcomes on a neutral and equal footing and remove the necessity of any presumed model or picture. We showcase the strategy’s generality and effectiveness on random long-range fermion and Kitaev spin liquid models [18], which lack a smoking-gun signature for quantum measurements. Especially, our strategy can work wonders even for complex states such as the disordered Kitaev QSL even with only non-repeating single-shot quantum measurements, fully capturing its non-Abelian topological degeneracy (Fig. 4). Indeed, every single-shot quantum measurement matters, as its outcome carries information. On the other hand, quantum-state reconstruction through measurements, often named quantum state tomography, has been a long-standing topic in quantum physics [38]. The recent introduction of neural-network-based tomography [39, 40] and shadow tomography [41] have achieved practical efficiency over multiple qubits. However, the neural networks are approximate, and the shadow tomography requires random tractable unitaries that can be hard to implement in general. Our strategy does not need such compromises.

The measurement energy —Consider the a-priori probability distribution $w(\Phi)$ of all quantum states $|\Phi\rangle$ spanning the Hilbert space, if a single-shot measurement of observable $\hat{O} = \sum_{\gamma} a_{\gamma} \hat{P}_{\gamma}$ yields an outcome $a_{\gamma'}$, the posterior probability after this measurement is:

$$w(\Phi) \rightarrow p(\Phi|\gamma') = p(\gamma'|\Phi)w(\Phi)/p(\gamma'), \quad (1)$$

where a_{γ} and \hat{P}_{γ} are the eigenvalues and the corresponding projection operators of the observable \hat{O} , $p(\gamma'|\Phi) = \langle \Phi|\hat{P}_{\gamma'}|\Phi\rangle$ is the probability of outcome $a_{\gamma'}$ given the quantum state $|\Phi\rangle$, and $p(\gamma')$ offers normalization [42].

As the measurements progress, we obtain a series of results $\mathcal{D} = \{\gamma_1, \gamma_2, \dots\}$ of single-shot measurements over observables $\{\hat{O}_1, \hat{O}_2, \dots\}$, and update the probability as:

$$w(\Phi) \propto \prod_{\gamma \in \mathcal{D}} p(\gamma|\Phi) = \prod_{\gamma \in \mathcal{D}} \langle \Phi|\hat{P}_{\gamma}|\Phi\rangle. \quad (2)$$

We define the ‘‘measurement energy’’:

$$E(\Phi) = - \sum_{\gamma \in \mathcal{D}} \log \langle \Phi | \hat{P}_\gamma | \Phi \rangle, \quad (3)$$

so that $w(\Phi) \propto \exp[-E(\Phi)]$ of a quantum state $|\Phi\rangle$ becomes analogous to a Boltzmann distribution with energy $E(\Phi)$ in unit of $k_B T$. Unlike the expectation value of a Hamiltonian of linear operators, the measurement energy $E(\Phi)$ is explicitly nonlinear due to the log function. Therefore, the probability distribution of a quantum state with measurement outcomes offers realizations of exotic nonlinear-operator Hamiltonian. We will show a protocol to locate the MLE states with minimum $E(\Phi)$.

The statistical meaning of Eq. 3 becomes clear in case of multiple measurements on the same observable \hat{O} , yielding N_γ instances of a_γ outcomes. By binning them together, we re-express the measurement energy as:

$$E(\Phi) = - \sum_{\gamma \in \mathcal{R}} N_\gamma \log \langle \Phi | \hat{P}_\gamma | \Phi \rangle = - \sum_{\gamma \in \mathcal{R}} N_{\hat{O}} f_\gamma \log \langle \Phi | \hat{P}_\gamma | \Phi \rangle, \quad (4)$$

which describes the cross entropy between the expected probability given a quantum state $|\Psi\rangle$ and the measured probability $f_\gamma = N_\gamma/N_{\hat{O}}$, further weighted by the number of measurements $N_{\hat{O}}$ on \hat{O} . Besides, the lower bound for measurement energy on given data is $\min(E) = - \sum_{\gamma \in \mathcal{R}} N_{\hat{O}} f_\gamma \log f_\gamma$, which makes $E(\Phi_0) - \min(E)$ a feasible indicator for satisfiability and convergence.

Measurement-energy minimums via iterative effective Hamiltonians —For a generic nonlinear cost function $E = f(\langle \hat{O} \rangle)$ defined for the expectation values $\langle \hat{O}_i \rangle = \langle \Phi | \hat{O}_i | \Phi \rangle$, its functional derivative with respect to $|\Phi\rangle$ should vanish at its minimum:

$$\delta E = \sum_i \left. \frac{\partial f(\langle \hat{O} \rangle)}{\partial \langle \hat{O}_i \rangle} \right|_{\langle \hat{O} \rangle_{gs}} \cdot \delta \langle \hat{O}_i \rangle_{gs} = 0, \quad (5)$$

where $\langle \hat{O}_i \rangle_{gs}$ are the expectation values at the minimum. We note that a Hamiltonian \hat{H}_{eff} on the same Hilbert space:

$$\hat{H}_{eff} = \sum_i \alpha_i \hat{O}_i, \quad (6)$$

should possess a ground state $|\Phi'_{gs}\rangle$ that satisfies $\delta \langle \hat{H}_{eff} \rangle = \sum_i \alpha_i \cdot \delta \langle \hat{O}_i \rangle_{gs} = 0$, which coincides with Eq. 5 if we set $|\Phi'_{gs}\rangle = |\Phi_{gs}\rangle$ and:

$$\alpha_i = \left. \frac{\partial f(\langle \hat{O} \rangle)}{\partial \langle \hat{O}_i \rangle} \right|_{\langle \hat{O} \rangle_{gs}}. \quad (7)$$

Eqs. 6 and 7 form a self-consistent equation for the minimum of measurement energy $E(\Phi)$.

Applying such protocol to the measurement energy in Eq. 3, the effective Hamiltonian is:

$$\hat{H}_{eff} = \sum_{\gamma \in \mathcal{R}} N_{\hat{O}} \alpha_\gamma \hat{P}_\gamma, \quad \alpha_\gamma = - \frac{f_\gamma}{\langle \Phi_{gs} | \hat{P}_\gamma | \Phi_{gs} \rangle}, \quad (8)$$

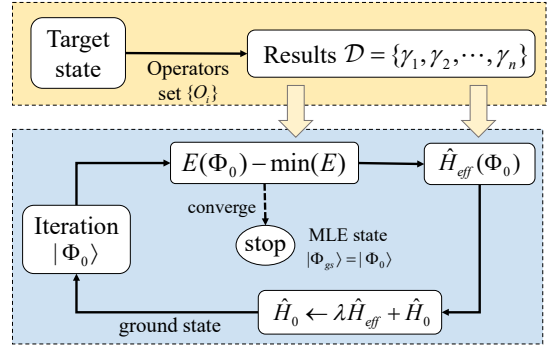


FIG. 1. We outline our strategy for the MLE quantum state: given the quantum measurement results, we iteratively update \hat{H}_0 with \hat{H}_{eff} and solve its ground state $|\Phi_0\rangle$, which converges to the MLE state $|\Phi_{gs}\rangle$. The measurement energy $E(\Phi_0) - \min(E)$ serves as an indicator of convergence and also reveals whether additional measurements and/or observables are preferable.

$f_\gamma = N_\gamma/N_{\hat{O}}$ and $N_{\hat{O}} = 1$ for single shots. Note that different observables may contribute to the same projection operator. Eq. 8 is one of the main conclusions of this letter: given the quantum measurements, the self-consistent ground state $|\Phi_{gs}\rangle$ of Eq. 8 is our MLE quantum state. However, as the iteration state approaches the target state, every $\langle \hat{P}_\gamma \rangle \rightarrow f_\gamma$, resulting a diminishing \hat{H}_{eff} and unstable eigenstates. Inspired by supervised machine learning [43–46], we regard \hat{H}_{eff} as a gradient and update the iteration model $\hat{H}_0 \rightarrow \hat{H}_0 + \lambda \hat{H}_{eff}$ as ‘‘quantum gradient descent’’, where the ground state $|\Phi_0\rangle$ of \hat{H}_0 converges to the MLE state $|\Phi_{gs}\rangle$. We summarize the strategy in Fig. 1, and discuss further details such as initialization \hat{H}_0 and gradient-descent rate λ in Ref. [47].

To see how \hat{H}_{eff} performs as a gradient, let’s consider a toy model where target state $|\Phi_t\rangle = \cos(\theta/2)|\uparrow\rangle + \sin(\theta/2)\exp(i\varphi)|\downarrow\rangle$ is a spin-1/2 spinor. The outcomes of a number $N_{\hat{O}}$ of $\hat{S}_z = \sigma^z/2$ measurements approach:

$$\lim_{N_{\hat{O}} \rightarrow \infty} N_{\pm} = N_{\hat{O}} \langle \Phi_t | \hat{P}_{\pm} | \Phi_t \rangle = N_{\hat{O}} \frac{(1 \pm \cos \theta)}{2}, \quad (9)$$

where $\hat{P}_{\pm} = (1 \pm \sigma^z)/2$ are the projection operators onto the $\sigma^z = \pm 1$ eigenspaces, respectively. For an iteration state current at $|\Phi_0\rangle = \cos(\theta'/2)|\uparrow\rangle + \sin(\theta'/2)\exp(i\varphi')|\downarrow\rangle$, $\alpha_{\pm} = -(1 \pm \cos \theta)/(1 \pm \cos \theta')$ contributes the following terms to the next \hat{H}_{eff} :

$$N_{\hat{O}}(\alpha_+ \hat{P}_+ + \alpha_- \hat{P}_-) = -N_{\hat{O}} \frac{\cos \theta - \cos \theta'}{1 - \cos^2 \theta'} \sigma^z + const. \quad (10)$$

It is straightforward to see that when $\theta' > \theta$ ($\theta' < \theta$), the coefficient of σ^z is negative (positive), giving preference to a smaller (larger) θ' for the next iteration, and so on so forth toward the target state. We also note that the \hat{S}_z

measurements provide no information on φ . Therefore, φ' remains its initial value unless there are φ -dependent measurements, such as on \hat{S}_x and \hat{S}_y .

It is high time we discussed the choices of observables \hat{O} , which play an essential role in terms of the projection operators \hat{P}_γ in Eq. 8. \hat{O} rely on the quantum systems and apparatus; fortunately, our strategy allows a joint interpretation across different platforms for a more comprehensive observable set. Importantly, a lack of observables may lead to misleading MLS states, which we can identify with signatures in measurement energy: it may constrain the search space leading to a sub-optimal MLE state as the measurement energy converges above its lower bound, or end up with different MLE states simultaneously consistent with the measurement outcomes. Also, an observable with more eigenvalues acts as a double-edged sword: they may incur cost in post-processing \hat{H}_{eff} due to more complex \hat{P}_γ , but also offer more information [48] - a distribution carries more information than the average, in a similar spirit to shot-noise studies [49, 50]. We will see examples later and in Ref. [47].

Example: random long-range fermion model—Let's consider the ground state of the following Hamiltonian:

$$\hat{H} = - \sum_{ij} t_{ij} (c_i^\dagger c_j + c_j^\dagger c_i) - \sum_i \mu_i c_i^\dagger c_i, \quad (11)$$

where $1 \leq i, j \leq L$. We apply random $t_{ij} \in [0, 1]$ between arbitrary sites and $\mu_i \in [-0.5, 0.5]$ to deny the system symmetries and locality. Still, our strategy can derive the target states, placed in a black box and tangible only via quantum measurements, even on relatively large systems. And we choose observables $\hat{O}_x = c_x^\dagger c_x$ and $\hat{O}'_{xy} = (c_x^\dagger + c_y^\dagger)(c_x + c_y)/2$ with eigenvalues $\{0, 1\}$, \hat{P}_γ and thus \hat{H}_{eff} remain fermion-bilinear, and $|\Phi_0\rangle$ can be obtained straightforwardly at each iteration.

For simplicity, we measure each observable $\hat{O} = \sum_\gamma \alpha_\gamma \hat{P}_\gamma$ on the target quantum state an equal number $N_{\hat{O}} \rightarrow \infty$ of times to suppress fluctuations, yielding $N_\gamma \rightarrow N_{\hat{O}} \times \langle \hat{P}_\gamma \rangle$ outcomes of α_γ respectively. Putting these results on $L = 100$ systems into the iterative process in Eq. 8, we obtain the results in Fig. 2. We observe a quick convergence of the iteration state $|\Phi_0\rangle$ towards the target state, its average measurement energy $E(|\Phi_0\rangle)$ towards lower bound [51].

More generally, our strategy also works for data laden with quantum fluctuations due to finite numbers of quantum measurements $N_{\hat{O}}$. Interestingly, $N_{\hat{O}}$ necessary for a certain fidelity level scales polynomially to the system size; see the inset of Fig. 2. We also study cases where $N_{\hat{O}}$ differs between observables [47]. Besides, we can measure \hat{O}_x and \hat{O}'_{xy} on a generic quantum many-body state, which constrains the iteration state $|\Phi_0\rangle$ to the search space of Hartree-Fock states. The corresponding results on the MLE states and measurement energies, summarized in Ref. [47], are consistent with our expect-

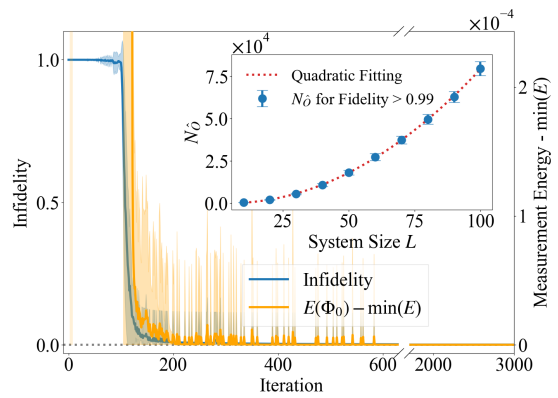


FIG. 2. Following our strategy, the iteration state $|\Phi_0\rangle$ quickly converges to the target quantum state (infidelity $\sim 6 \times 10^{-4}$), and the average measurement energy $E(|\Phi_0\rangle)$ converges to its lower bound. The shade is based upon 100 trials on different target states, the ground states of long-range fermion models with system size $L = 100$. The inset illustrates the number of measurements $N_{\hat{O}}$ needed for fidelity > 0.99 versus different system sizes L . The error bars are based on 50 trials, and the red dashed curve shows a quadratic fit.

tations.

Example: strongly-correlated Kitaev QSL state—Let's consider the nearest-neighbor spin Hamiltonian on the honeycomb lattice:

$$\hat{H} = \sum_{\langle ij \rangle \in \alpha\beta(\gamma)} \left[J \vec{S}_i \cdot \vec{S}_j + K S_i^\gamma S_j^\gamma + \Gamma (S_i^\alpha S_j^\beta + S_i^\beta S_j^\alpha) \right], \quad (12)$$

which potentially describes the Kitaev physics in the A_2IrO_3 -family iridates [52] and Kitaev material $RuCl_3$ [20]. K , J , and Γ are the amplitudes of the Kitaev interaction, isotropic Heisenberg interaction, and the symmetric off-diagonal interactions, respectively. Depending on the bond dimension, each bond is labeled by $\alpha\beta(\gamma)$, where $\gamma = x, y, z$ is the spin direction in the Kitaev term, and α, β are the two orthogonal spin directions in the Γ term. The pristine Kitaev model ($J = \Gamma = 0$) is analytically solvable [18, 47]. We take the ground state of \hat{H} with a dominant Kitaev term on a 3×3 system with periodic boundary condition, illustrated in the inset of Fig. 3(b), as our target quantum state. The resulting QSL states are notorious for their lack of smoking-gun signatures. Instead, we probe the target quantum states with *seemingly trivial* quantum measurements. As we will see, these measurements still provide insightful information, and our strategy leads to the target states and, in turn, their abstract natures, including QSL phase [7–9] and quantum entanglements [2–6].

To begin with, we set $K = -1$, $J = 0.1$. Given the C_3 rotation symmetry, there are three degenerate ground states, shown in the inset of Fig. 3(a). These ground states are topologically degenerate with no quasiparticles [18, 29, 47, 53]. Here, we consider quantum measure-

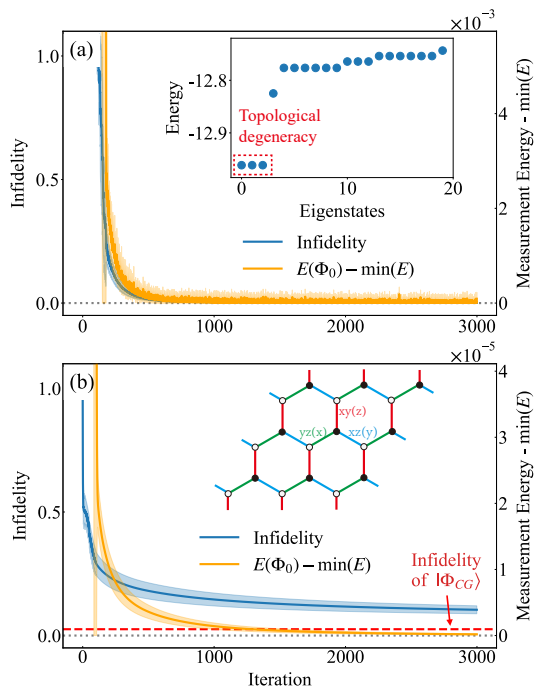


FIG. 3. (a) We apply our strategy to the quantum-measurement outcomes of $\sigma_i^\lambda \sigma_j^\lambda$, $\lambda = x, y, z$, on one of the ground states of Eq. 12 with $K = -1$, $J = 0.1$, and $\Gamma = 0$ (spectrum in the inset), the measurement energy $E(\Phi_0)$ quickly saturates the lower bound, while the iteration states $|\Phi_0\rangle$ converge to the target state with infidelity $\sim 10^{-3}$. (b) With the same measurements on the ground states for $K = 1$, $J = 0.1$, and $\Gamma \in [0, 0.1]$, the measurement energy $E(\Phi_0)$ still quickly saturates the lower bound, while the MLE states $|\Phi_{gs;trial}\rangle$ show slight infidelity ~ 0.1 with the target state and differ between trials with average overlap ~ 0.83 . The red dashed line shows the state $|\Phi_{CG}\rangle$ averaged over multiple trials [47], which offers an improved approximation with infidelity ~ 0.03 . The shades are based on multiple trials with different initializations. The inset in (b) is a sketch of the Kitaev model on a 3×3 honeycomb lattice.

ments on simple observables $\sigma_i^\lambda \sigma_j^\lambda$ of each $\langle ij \rangle$ bond on one of the ground states, $\lambda = x, y, z$. Similar quantum measurements are potentially available to QSL models in Rydberg-atom systems [54–56], or via electron-spin-resonance scanning tunneling microscopy experiments [57, 58], etc. In the large $N_{\mathcal{O}} \rightarrow \infty$ limit, we obtain $N_{\pm}(ij, \lambda) = N_{\mathcal{O}} \times \langle \hat{P}_{\pm}(ij, \lambda) \rangle$ counts of ± 1 outcomes, $\hat{P}_{\pm}(ij, \lambda) = (1 \pm \sigma_i^\lambda \sigma_j^\lambda)/2$, respectively. Putting these results into the iterations in Eq. 8, $|\Phi_0\rangle$ successfully converges to the target ground-state manifold, see Fig. 3(a). Interestingly, starting from a single ground state, we possess the entire topologically degenerate manifold with high fidelity [47], with which we can achieve fundamental properties such as quasiparticle statistics [7–9]. On the one hand, these states share identical local properties thus equal qualifications for the MLE states; on the other hand, their simultaneous presence implies that

\hat{H}_0 inherits topological information already present in the target state.

Another interesting scenario is when the observables involved are insufficient to locate the target state fully, as multiple states saturate the measurement energy to the lower bound. For example, we consider the ground state of $K = 1$, $J = 0.1$, and random $\Gamma \in [0, 0.1]$ on each bond. The system possesses a unique ground state without topological degeneracy on a 3×3 system [47]. We keep our observables $\sigma_i^\lambda \sigma_j^\lambda$, $\lambda = x, y, z$ and a large number $N_{\mathcal{O}} \rightarrow \infty$ of quantum measurements as before, whose results on 10 independent trials are summarized in Fig. 3(b). While all trials converge fully and leave little measurement-energy residue, the obtained MLE states $|\Phi_{gs;trial}\rangle$ differ from trial to trial, with an average overlap ~ 0.83 in between. We cannot further distinguish these states, which satisfy the quantum measurements equally, until additional observables for further information. Also, we may seek common ground $|\Phi_{CG}\rangle$ between $|\Phi_{gs;trial}\rangle$ as a contingency plan in case of limited ambiguity; see the red dashed line in Fig. 3(b) and details in Ref. [47].

Finally, we consider an unprecedented scenario to showcase the adaptability of our strategy: the observables on nearest-neighbor bonds are $\sigma_i^{\hat{n}} \sigma_j^{\hat{n}}$ for random \hat{n} directions and measured once each. Such single-shot results, a list of ± 1 outcomes, are plagued with ultimate fluctuations and hard to make use of; nevertheless, our strategy can capitalize on their intrinsic information and unravel the underlying target state. To further increase the challenge, we pick disordered non-Abelian topologically ordered states by setting $K = -1$ and random $J \in [0, 0.1]$, $\Gamma \in [0, 0.3]$ on each bond for our target quantum many-body states, whose topological properties are analyzed in detail in Ref. [47]. We summarize the demonstration in Fig. 4: the more single shots, the more information at disposal, and the higher the fidelity of the MLE states $|\Phi_{gs}\rangle$; based on a single quantum state, we also obtain the degenerate manifold with high fidelity with the originals [59]. We emphasize that although our setup resembles the shadow tomography [60], it does not satisfy the prerequisite randomness of the latter. Indeed, our strategy is more generally applicable and does not rely on the randomness, or any other scheme, of the measurements.

Discussions —In addition to our iterative effective-Hamiltonian approach, one may also optimize states variationally for Eq. 3 as the cost function. However, the chosen ansatz may constrain the search, e.g., the matrix product states cannot capture the random long-range fermion states due to locality [61]. While our strategy is more general, there may be barriers when the effective Hamiltonian takes a strongly-correlated form in practice. One may need numerical methods such as exact diagonalization, density-matrix renormalization group [62, 63], quantum Monte Carlo methods [64, 65], or a quantum

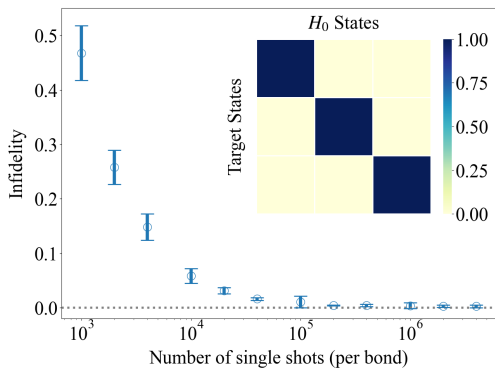


FIG. 4. Single-shot quantum measurements $\sigma_i^{\hat{n}}\sigma_j^{\hat{n}}$ for random \hat{n} directions yield a list of fluctuation-laden ± 1 . Based upon such single-shot outcomes from non-Abelian topologically ordered ground states with $K = -1$, $J \in [0, 0.1]$, $\Gamma \in [0, 0.03]$ in the Kitaev model in Eq. 12, our strategy allows the MLE states to converge asymptotically well to the target states within 1500 iterations as the number of single shots increases. The error bars are based on ten different trials. The inset demonstrates the fidelity between the lowest three eigenstates of the iteration \hat{H}_0 at convergence and the topological degenerate states of the target system.

simulator that evaluates the expectation values of Eq. 8 [66–68].

We observe that the final \hat{H}_0 is not necessarily connected with the target state’s original Hamiltonian, if available. Indeed, the mapping between Hamiltonians and eigenstate is many-to-one. Interestingly, such \hat{H}_0 also paves the way for parent Hamiltonian reconstruction [69, 70]. \hat{H}_0 may differ from trial to trial given the gradient-descent nature and different initializations, allowing exploration for universality.

Considering the exponentially large Hilbert space of a quantum many-body system, we have offered a quantum strategy to interpret quantum measurements in a general and precise way. We note that the additive form of the measurement energy in Eq. 3 means that *every single-shot quantum measurement counts*. On the other hand, for cases where the measurement outcomes \mathcal{D} are not directly obtainable, we can reverse engineer values of f_γ from the expectation values $\langle \hat{O} \rangle$, $\langle \hat{O}^2 \rangle$, \dots [36], and $N_{\hat{O}}$ as a confidence measure. The strategy can also be generalized to target mixed states represented by density operators, while generalization to quantum measurements connecting ground state and excited states, e.g., inelastic spectroscopy experiments, remains an open question for future research.

Acknowledgement: We acknowledge helpful discussions with Zhen-Duo Wang, Tian-Lun Zhao, Pei-Lin Zheng, Hao-Yan Chen, and Yuan Wan. We also acknowledge support from the National Science Foundation of China (No.12174008) and the National Key R&D Program of China (No.2021YFA1401900). The calculations

of this work are supported by HPC facilities at Peking University.

* frankzhangyi@gmail.com

- [1] J. Quintanilla and C. Hooley, *Physics World* **22**, 32 (2009).
- [2] A. Kitaev and J. Preskill, *Phys. Rev. Lett.* **96**, 110404 (2006).
- [3] M. Levin and X.-G. Wen, *Phys. Rev. Lett.* **96**, 110405 (2006).
- [4] X. Chen, Z.-C. Gu, and X.-G. Wen, *Phys. Rev. B* **82**, 155138 (2010).
- [5] Y. Zhang, T. Grover, and A. Vishwanath, *Phys. Rev. B* **84**, 075128 (2011).
- [6] Y. Zhang, T. Grover, and A. Vishwanath, *Phys. Rev. Lett.* **107**, 067202 (2011).
- [7] Y. Zhang, T. Grover, A. Turner, M. Oshikawa, and A. Vishwanath, *Phys. Rev. B* **85**, 235151 (2012).
- [8] T. Grover, Y. Zhang, and A. Vishwanath, *New Journal of Physics* **15**, 025002 (2013).
- [9] Y. Zhang, T. Grover, and A. Vishwanath, *Phys. Rev. B* **91**, 035127 (2015).
- [10] F. D. M. Haldane, *Phys. Rev. Lett.* **61**, 2015 (1988).
- [11] R. B. Laughlin, *Phys. Rev. Lett.* **50**, 1395 (1983).
- [12] C. L. Kane and E. J. Mele, *Phys. Rev. Lett.* **95**, 146802 (2005).
- [13] M. Z. Hasan and C. L. Kane, *Rev. Mod. Phys.* **82**, 3045 (2010).
- [14] H. Nielsen and M. Ninomiya, *Physics Letters B* **130**, 389 (1983).
- [15] X. Yuan, C. Zhang, Y. Zhang, Z. Yan, T. Lyu, M. Zhang, Z. Li, C. Song, M. Zhao, P. Leng, M. Ozerov, X. Chen, N. Wang, Y. Shi, H. Yan, and F. Xiu, *Nature Communications* **11**, 1259 (2020).
- [16] B. Keimer and J. E. Moore, *Nature Physics* **13**, 1045 (2017).
- [17] A. Kitaev, *Annals of Physics* **303**, 2 (2003).
- [18] A. Kitaev, *Annals of Physics* **321**, 2 (2006).
- [19] S. Yan, D. A. Huse, and S. R. White, *Science* **332**, 1173 (2011).
- [20] A. Banerjee, C. A. Bridges, J.-Q. Yan, A. A. Aczel, L. Li, M. B. Stone, G. E. Granroth, M. D. Lumsden, Y. Yiu, J. Knolle, S. Bhattacharjee, D. L. Kovrizhin, R. Moessner, D. A. Tennant, D. G. Mandrus, and S. E. Nagler, *Nature Materials* **15**, 733 (2016).
- [21] J. G. Bednorz and K. A. Müller, *Zeitschrift für Physik B Condensed Matter* **64**, 189 (1986).
- [22] Y. Kamihara, H. Hirano, R. Kawamura, H. Yanagi, T. Kamiya, and H. Hosono, *Journal of the American Chemical Society* **128**, 10012 (2006).
- [23] Y. Kamihara, T. Watanabe, M. Hirano, and H. Hosono, *Journal of the American Chemical Society* **130**, 3296 (2008).
- [24] Y. Cao, V. Fatemi, S. Fang, K. Watanabe, T. Taniguchi, E. Kaxiras, and P. Jarillo-Herrero, *Nature* **556**, 43 (2018).
- [25] K. v. Klitzing, G. Dorda, and M. Pepper, *Phys. Rev. Lett.* **45**, 494 (1980).
- [26] D. C. Tsui, H. L. Stormer, and A. C. Gossard, *Phys. Rev. Lett.* **48**, 1559 (1982).

- [27] F. D. M. Haldane, Phys. Rev. Lett. **50**, 1153 (1983).
- [28] K. von Klitzing, Rev. Mod. Phys. **58**, 519 (1986).
- [29] X. G. Wen and Q. Niu, Phys. Rev. B **41**, 9377 (1990).
- [30] F. D. M. Haldane, Phys. Rev. Lett. **93**, 206602 (2004).
- [31] B. A. Bernevig, T. L. Hughes, and S.-C. Zhang, Science **314**, 1757 (2006).
- [32] L. Fu, C. L. Kane, and E. J. Mele, Phys. Rev. Lett. **98**, 106803 (2007).
- [33] X. Chen, Z.-C. Gu, Z.-X. Liu, and X.-G. Wen, Science **338**, 1604 (2012).
- [34] E. Fradkin, S. A. Kivelson, and J. M. Tranquada, Rev. Mod. Phys. **87**, 457 (2015).
- [35] C. Proust and L. Taillefer, Annual Review of Condensed Matter Physics **10**, 409 (2019).
- [36] J. J. Sakurai and J. Napolitano, *Modern quantum mechanics; 2nd ed.* (Addison-Wesley, San Francisco, CA, 2011).
- [37] T.-H. Han, J. S. Helton, S. Chu, D. G. Nocera, J. A. Rodriguez-Rivera, C. Broholm, and Y. S. Lee, Nature **492**, 406 (2012).
- [38] A. I. Lvovsky and M. G. Raymer, Rev. Mod. Phys. **81**, 299 (2009).
- [39] G. Torlai, G. Mazzola, J. Carrasquilla, M. Troyer, R. Melko, and G. Carleo, Nature Physics **14**, 447 (2018).
- [40] J. Carrasquilla, G. Torlai, R. G. Melko, and L. Aolita, Nat. Mach. Intell. **1**, 155 (2019).
- [41] H.-Y. Huang, R. Kueng, and J. Preskill, Nature Physics **16**, 1050 (2020).
- [42] F. Huszár and N. M. Houlby, Physical Review A **85**, 052120 (2012).
- [43] Michael Nielsen, *Neural Networks and Deep Learning* (Free Online Book, 2013).
- [44] J. Carrasquilla and R. G. Melko, Nature Physics **13**, 431 (2017).
- [45] Y. Zhang and E.-A. Kim, Phys. Rev. Lett. **118**, 216401 (2017).
- [46] Y. Zhang, A. Mesaros, K. Fujita, S. Edkins, M. Hamidian, K. Ch'ng, H. Eisaki, S. Uchida, J. S. Davis, E. Khatami, *et al.*, Nature **570**, 484 (2019).
- [47] See examples and details on hyper-parameters, finite number of measurements, interacting fermion models, topological degeneracy of the Kitaev model, contingency plan for insufficiency observables in Supplemental Materials, which also include Ref. ? ? ? ? ? ? ? ? .
- [48] We can make an observable simpler to handle by binning together some of its outcomes and gives up some part of its information, but not vice versa.
- [49] P. Zhou, L. Chen, Y. Liu, I. Sochnikov, A. T. Bollinger, M.-G. Han, Y. Zhu, X. He, I. Bozovic, and D. Natelson, Nature **572**, 493 (2019).
- [50] E. Sivre, H. Duprez, A. Anthore, A. Aassime, F. D. Parmentier, A. Cavanna, A. Ouerghi, U. Gennser, and F. Pierre, Nature Communications **10**, 5638 (2019).
- [51] The spikes in the figure are mainly due to the inconsistent particle number the iteration state $|\Phi_0\rangle$ receives over the slight modifications.
- [52] J. G. Rau, E. K.-H. Lee, and H.-Y. Kee, Phys. Rev. Lett. **112**, 077204 (2014).
- [53] M. B. Hastings and X.-G. Wen, Phys. Rev. B **72**, 045141 (2005).
- [54] R. Verresen, M. D. Lukin, and A. Vishwanath, Phys. Rev. X **11**, 031005 (2021).
- [55] G. Semeghini, H. Levine, A. Keesling, S. Ebadi, T. T. Wang, D. Bluvstein, R. Verresen, H. Pichler, M. Kalinowski, R. Samajdar, A. Omran, S. Sachdev, A. Vishwanath, M. Greiner, V. Vuletić, and M. D. Lukin, Science **374**, 1242 (2021).
- [56] R. Samajdar, W. W. Ho, H. Pichler, M. D. Lukin, and S. Sachdev, Proceedings of the National Academy of Sciences **118**, e2015785118 (2021), <https://www.pnas.org/doi/pdf/10.1073/pnas.2015785118>.
- [57] A. V. Balatsky, M. Nishijima, and Y. Manassen, Advances in Physics **61**, 117 (2012).
- [58] M. Ternes, New Journal of Physics **17**, 063016 (2015).
- [59] Note that a measurement-energy lower bound is no longer available for such single-shot measurements.
- [60] H.-Y. Huang, R. Kueng, and J. Preskill, Nature Physics **16**, 1050 (2020).
- [61] U. Schollwöck, Annals of Physics **326**, 96 (2011).
- [62] M. Fannes, B. Nachtergaele, and R. F. Werner, Communications in Mathematical Physics **144**, 443 (1992).
- [63] U. Schollwöck, Rev. Mod. Phys. **77**, 259 (2005).
- [64] W. M. C. Foulkes, L. Mitas, R. J. Needs, and G. Rajagopal, Rev. Mod. Phys. **73**, 33 (2001).
- [65] M. Troyer and U.-J. Wiese, Phys. Rev. Lett. **94**, 170201 (2005).
- [66] E. Farhi, J. Goldstone, and S. Gutmann, "A quantum approximate optimization algorithm," (2014), arXiv:1411.4028 [quant-ph].
- [67] L. Zhou, S.-T. Wang, S. Choi, H. Pichler, and M. D. Lukin, Phys. Rev. X **10**, 021067 (2020).
- [68] P. Vikstål, M. Grönkvist, M. Svensson, M. Andersson, G. Johansson, and G. Ferrini, Phys. Rev. Applied **14**, 034009 (2020).
- [69] X.-L. Qi and D. Ranard, Quantum **3**, 159 (2019).
- [70] X. Turkeshi, T. Mendes-Santos, G. Giudici, and M. Dalmonde, Phys. Rev. Lett. **122**, 150606 (2019).